High-speed tomography of time-bin-entangled photons using a single-measurement setting

S. X. Wang,[1] C. Chan,[1] P. Moraw,[1] D. R. Reilly,[1] J. B. Altepeter,[2] and G. S. Kanter[1]
[1]*NuCrypt, LLC, 1840 Oak Ave., Suite 212-S, Evanston, Illinois 60201, USA*
[2]*Center for Photonic Communication and Computing, EECS Department, Northwestern University, 2145 Sheridan Road, Evanston, Illinois 60208, USA*
(Received 24 July 2012; published 25 October 2012)

We generate time-bin entangled photons and measure the resulting quantum state with a tomography system that uses asymmetric interferometers having 3 × 3 output couplers. This configuration allows for measurements to be made simultaneously in all bases that are required for tomographic reconstruction. By eliminating the burden of tuning interferometer phases and by measuring all the spatial and temporal modes, substantial improvements in measurement speed are observed. Raw fidelities of 84% with respect to an ideal entangled state are measured in about 2 s using a 12-MHz entangled state generator, with corresponding accidental count subtracted fidelities exceeding 90%.

DOI: 10.1103/PhysRevA.86.042122 PACS number(s): 03.65.Wj, 42.50.Ar, 03.65.Ud

I. INTRODUCTION

Entanglement is a fundamental resource in quantum information. Entangled photons are the most practical means of distributing entanglement over long distances, in part due to the availability of low-loss fiber optical cable. Numerous polarization-entangled photon pair sources have been constructed, and they are often characterized, using quantum state tomography (QST) [1,2]. QST is a measurement protocol that enables complete reconstruction of an unknown quantum state's density matrix using photon statistics measured in multiple bases both singly and in coincidence [3]. Polarization-based QST has recently been performed on photons subject to fiber polarization mode dispersion [4] and also at near real-time speeds [5]. Polarization entangled states are easily manipulated by widely available polarization control components. At least nine different measurement configurations (all combinations of three different bases for the signal and idler) are required for a complete polarization tomography, although in practice 36 measurements are often recorded since the redundant measurements make the state reconstruction more robust to certain experimental nonidealities, such as bases-dependent detection efficiency [6,7].

In principle it is possible to make measurements in all necessary bases simultaneously by splitting the polarization-entangled signal and idler photons into multiple paths and measuring each path in a different basis (effectively performing a tomographically complete positive-operator valued measurement or POVM [8]). This technique would consume a substantial amount of resources; in practice the basis states are usually cycled over time and collected into an equivalent single measurement in postprocessing. One drawback of polarization entanglement is the unknown and often unstable polarization transfer function experienced when distributing the entangled photons over long lengths of fiber, although it is possible to design systems with polarization tracking mechanisms to account for such polarization drift [9]. In a tomography measurement it is also possible to account for a fixed polarization transfer function via software processing; in this case the polarization transfer function must still be stable over each full set of tomography measurements.

Another option for dealing with the unstable fiber polarization transformation is to abandon polarization entanglement and instead encode the same quantum state into a degree of freedom not affected by these polarization drifts. A common polarization-insensitive degree of freedom is the temporal degree of freedom [10–12]. "Time-bin" entangled states exhibit quantum correlations between two temporal modes. In most applications, the temporal modes are measured by using an asymmetric Mach-Zehnder interferometer, creating three relevant time modes. The first and third temporal modes exhibit correlations independent of the interferometer's phase, while the central temporal mode or "energy mode" has correlations that depend on the bias phases of the signal and idler photon interferometers. The interferometer phases need to be stable and controllable, which can be achieved for instance by using temperature-controlled integrated optical interferometer circuits [12]. In an alternative arrangement the time-bin entanglement can be converted into polarization entanglement at the receivers [13]; however this still requires some level of polarization tracking.

Several experiments have used time-bin entanglement for quantum cryptography or for violating Bell's inequalities [11,13,14]. However, to the best of our knowledge there is only one time-bin QST that has been reported [12]. This time-bin QST experiment measured all three temporal modes using a high speed GHz-gated detector which allowed the closely spaced temporal modes associated with integrated interferometers to be distinguished. This implies that both time and energy bases are recorded together. However, measuring in these three time bins is insufficient for a complete tomography. A full tomography requires two additional bias phase settings for each of the two interferometers in order to span the energy basis, or a total of four bias phase pairs. The use of thermally tuned integrated optical interferometers can make tuning the bias phase relatively slow. Also, a single universal measurement is inherently appealing since it is more robust against systematic errors which occur on the same time scale as individual tomographic basis measurements, for example, if the state is drifting or being manipulated by a third party.

Time-bin tomography has the disadvantage that for a given detector time resolution (or analogously a given maximum

pulse repetition rate), the clock rate for entangled pair production and measurement is reduced by the number of time bins (typically three). Additionally, the number of dark counts during the pair measurement is correspondingly increased. However, one advantage of time-bin tomography heretofore not leveraged is that multiple central time bins with different bias phases can be simultaneously generated when using non-50:50 couplers at the output of the asymmetric interferometer. For instance, optical hybrids or simple 3×3 couplers can be used to create multiple outputs with different effective interferometer bias phases. By using such an interferometer and measuring all output ports in all time bins, a complete tomography can be performed without adjusting the interferometer bias phase. Changing the output coupler is more resource efficient than using a splitter followed by multiple independent interferometers.

In this paper we report on a time-bin tomography measurement that uses phase-stabilized fiber-based asymmetric Mach-Zehnder interferometers with 3×3 output couplers. All temporal modes in all output ports are simultaneously measured allowing for complete tomographic reconstruction using a single bias phase value for each interferometer. This method is useful for quickly characterizing quantum systems subject to time-dependent systematic effects from either environmental causes or due to malicious third parties. Although our detector gate rate is limited to 47 MHz, we can measure complete time-bin tomographies of high quality in about 2 s of contiguous data collection time, which is well over an order of magnitude faster than previous time-bin tomography experiments [12].

II. BACKGROUND

Consider a pair of isolated pump pulses generating correlated photons via a nonlinear process, such a four wave mixing [15]. The dual pumps define two time bins separated by the interslot time τ, which we label $|0\rangle$ and $|1\rangle$. Roughly speaking the signal and idler photon pairs are both generated in either the $|0\rangle$ or $|1\rangle$ time slot. The signal and idler are distinguishable based on wavelength and are each directed to a different asymmetric interferometer for measurement. The measurement interferometers split the input photon into two arms, delay one arm by τ with respect to the other and finally interfere the signals in the two arms by coupling them using two inputs of a 3×3 fused fiber coupler. The 3×3 coupler acts as a projective measurement with nine outputs when applied to a temporal qubit (three output time bins for each of three output spatial modes). Three output time slots are created in each of the three output ports of this coupler. Regardless of spatial mode, the first and third output time slots act as projective measurements of the states $|0\rangle$ and $|1\rangle$, respectively. In other words, only a photon generated in time slot $|0\rangle$ can be detected in the first output time slot and only a photon generated in time slot $|1\rangle$ can be detected in the third output time slot. The first (third) time slot is measured by summing the output of the first (third) time slot on all three interferometer output ports. Photons in the second output time slot in output ports A, B, and C are subject to projective

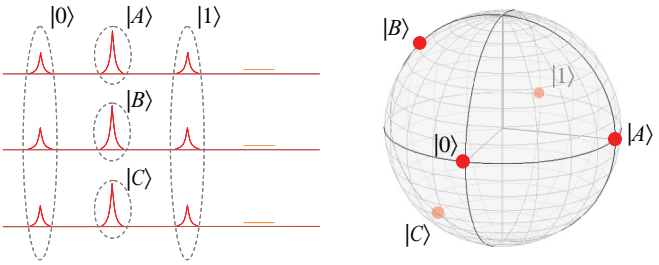

FIG. 1. (Color online) (a) Illustration of the four time bins on each of the three interferometer output ports and the respective projective measurements. One time bin is intentionally left empty for diagnostic purposes. (b) Poincaré sphere representation of the same measurements.

measurements in the states

$$|A\rangle = \frac{|0\rangle + e^{i(\Phi_k)}|1\rangle}{\sqrt{2}}, \tag{1}$$

$$|B\rangle = \frac{|0\rangle + e^{i(\Phi_k + \frac{2\pi}{3})}|1\rangle}{\sqrt{2}}, \tag{2}$$

$$|C\rangle = \frac{|0\rangle + e^{i(\Phi_k + \frac{4\pi}{3})}|1\rangle}{\sqrt{2}}, \tag{3}$$

respectively, where Φ_k is the phase bias of interferometer k and the subscript $k = s$ or i designates the signal or idler photons, respectively. The correlations between the $|A\rangle$, $|B\rangle$, and $|C\rangle$ modes of the two interferometers depend on the bias phase setting of the signal and idler interferometers, Φ_s and Φ_i, respectively, analogous to the more traditional situation where 2×2 couplers are used [12]. The projective measurements performed by the possible spatial and temporal mode locations of one interferometer are illustrated in Fig. 1(a). This arrangement produces five separate measurements for each interferometer. The projective measurements are also illustrated using positions on the Poincaré sphere in Fig. 1(b) [7], showing that the five states fully span the Stokes space. The photon count results from every combination of the five separate measurements are correlated, yielding 25 different coincidence count values for a given tomography.

The five measurements $\{|0\rangle,|1\rangle,|A\rangle,|B\rangle,|C\rangle\}$ and their respective 25 correlated measurements,

$$\begin{aligned} &\{|0\rangle,|1\rangle,|A\rangle,|B\rangle,|C\rangle\}_{\text{signal}} \\ &\otimes \{|0\rangle,|1\rangle,|A\rangle,|B\rangle,|C\rangle\}_{\text{idler}}, \end{aligned} \tag{4}$$

are informationally complete [4] and thus contain all the necessary information for complete quantum state tomography. Thus, a complete tomography in principle requires only that the bias phase of the two measurement interferometers be stabilized. In practice, however, the efficiencies of the single-photon detectors used to measure the photons at each of the output ports will be different and the pair-production rate of the entangled photon source will in general be unknown. In order to make an accurate reconstruction the set of measurements should allow the detector efficiencies and pair production rate to be estimated directly. These estimations can be made fairly accurately using just one bias phase setting on each of the interferometers (one bias phase

pair) provided that the input state possesses a high degree of symmetry, such as the maximally entangled state that our entangled source is configured to generate. This allows the system to accurately reconstruct an unknown state using only a single interferometer bias phase pair and without requiring calibration on all six detectors. More generally, one can make an initial set of measurements with each interferometer set to three different bias phase values which vary by 120° (for a total of $3 \times 3 = 9$ different bias phase pair settings) in order to calibrate the overall relative detection efficiencies, or alternatively, the detection efficiencies of each of the detectors can be made by comparing the singles counts using a fixed stable optical input power.

III. EXPERIMENT

A schematic of the experiment is shown in Fig. 2. A 47-Mega-pulse-per-second (Mpps) 1554.2-nm mode-locked laser (Polaronyx Mercury) is used as the pump source. A series of 100-GHz dense wavelength division multiplexing (DWDM) filters define the shape of the pump spectrum with a >120 dB extinction ratio. The pump source then passes through a >30 dB extinction ratio amplitude modulator, driven by an 11.75-MHz square wave produced by dividing the repetition frequency of the laser by four to produce an on-on-off-off pulse pattern, shown in the scope capture in the left inset of Fig. 2. The {1,1,0,0} pump pulse pattern creates four time bins, with the fourth time bin being an empty bin (containing no light after the detection interferometer) that is used only for diagnostic purposes. The generation and detection rate could be improved by 33% by using a {1,1,0} pattern having three time bins for each entangled state. As configured, entangled states (pump pulse pairs) are generated at an 11.75-MHz rate. It is unusual for a mode-locked laser to directly create the pulse pairs and it requires the laser have high pulse-to-pulse coherence. More typically pulse pairs are generated by passing a single laser pulse through an asymmetric interferometer [11,13,14] or by directly carving a cw laser [12,15]. In our experiment simply passing two mode-locked laser pulses directly required the minimum number of resources.

The pump pulse pairs are coupled to a 300-m dispersion shifted fiber (DSF) in order to generate temporally correlated signal and idler photon pairs via four-wave-mixing [15]. In order to reduce noise photons due to Raman scattering, the DSF is cooled inside a freezer to −80 °C. The signal and idler photons are separated via a wavelength division multiplexing (WDM) add-drop multiplexer (ADM), then input into their

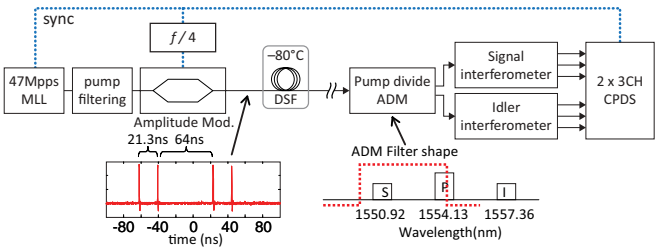

FIG. 2. (Color online) Schematic diagram of the time-bin entanglement system setup. Left inset: scope capture of the pump source. Right inset: illustrated ADM filter shape.

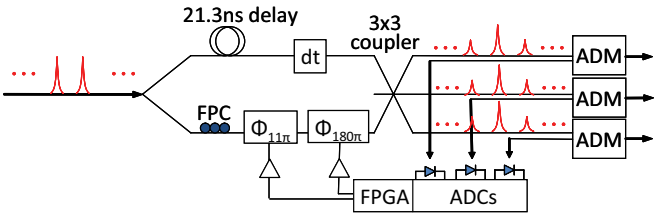

FIG. 3. (Color online) Diagram of the 3 × 3 asymmetric interferometer with active phase locking.

respective 1-bit delay interferometers. The ADM has a cutoff near the pump wavelength, which allows a portion of the pump source to be split into both the signal and idler interferometers as illustrated in the right inset of Fig. 2. Because the pump source is phase stable with both the signal and the idler photons produced, it can be extracted after each interferometer and used as reference signal to stabilize and control the bias phase. The signal and idler outputs of the interferometers are photon counted and correlated using a correlated photon detection system (NuCrypt CPDS-1000) modified so that the 10 singles counts and 25 coincidences described previously can be measured. The quantum state tomography analysis is then performed offline on a separate computer.

A schematic of the 1-bit-delay interferometer is shown in Fig. 3. One arm of the interferometer contains a fiber polarization controller (FPC) followed by two phase shifters. Each phase shifter is driven by the amplified output of a 12-bit digital to analog converter (DAC) that is controlled by a field programmable gate array (FPGA). The smaller phase shifter with 11π range is used for high resolution phase adjustments and a larger range phase shifter with more than 180π of range is added to cover slow but large magnitude long-term phase drift due to temperature variations. The FPC aligns the polarization of the two arms at the output for maximal interference. The other interferometer arm contains a fiber patch cord that provides a one pulse delay (21.3 ns). The insertion losses of the two arms are matched to within 2%. The output coupler of the interferometer is a 3 × 3 fused fiber coupler, with the combining phase of the arms nominally 120° apart from each other. Using a 3 × 3 coupler eliminates the phase-to-amplitude ambiguity inherent in a 180° 2 × 2 coupler, thus allowing the interferometer to be set and stabilized at any specified phase by locking the output amplitude ratios of the three outputs.

Due to the long (21.3 ns) asymmetric time delay required in the interferometer matched to the 47-MHz pulse repetition rate, active phase locking is necessary to make useful measurements. To set the interferometer to the desired phase positions, we use the residual pump source as a reference signal. The residual pump power from each of the output ports of the interferometer is extracted by the ADMs and monitored using an analog to digital converter (ADC). Perfect interference is not expected in the residual pump because interference occurs only in the energy bins. Ideally there are three locking points where the power in two out of the three interferometer output ports are set to be equal and each of these locking points have bias phases that differ by 120°. Imperfect interference and mismatches in overall signal gain are accounted for by an initial calibration where the signal in each ADC is simultaneously monitored as the interferometer phase is scanned over a full 2π range.

An FPGA stores the calibration information and controls the voltage sent to the interferometer phase shifters. The ditherless locking method also has the capability of locking to phase values other than the 120° steps described here, but that function is not necessary for this experiment.

Each of the 3×3 output arms on both interferometers are measured by a different single-photon detector (SPD). Differing losses in the optical paths of the interferometer as well as differing quantum efficiencies of the individual SPDs will result in a different overall quantum efficiency for each interferometer output port. Once measured, these efficiencies can be incorporated into a tomographic reconstruction algorithm [6]. To perform a robust measurement of these efficiencies in real time, we can subject each detector to a set of nine different measurement settings corresponding to every combination of $\Phi_{S,i} = \{0°,120°,240°\}$. The total coincidence counts involving each of the six detectors spread over all nine measurement settings will be proportional to the detector's quantum efficiency η. Once measured, these six values for η can be used together with the 25 coincidence count totals from a single measurement setting to reconstruct an unknown input quantum state, regardless of the relative detector efficiencies.

The state reconstruction algorithm is a modified version of the recently developed linear-least-squares technique [5]. This method uses the 2-qubit Stokes vector as a linear model, and solves the least-squares problem $w\mathbf{M}\cdot\mathbf{S} = w\mathbf{C}$. Here, $\mathbf{M}$ is a matrix containing the set of measurements derived from the twenty-five coincidence count measurement and weighted using the detector efficiencies; $\mathbf{C}$ is a vector containing the measured singles counts; $\mathbf{S}$ is the Stokes vector representing the unknown state; and w is a weight vector representing the distribution width for each measurement. We assume the counting process is Poissonian and in the large-N limit where the Poisson distribution is approximated as a Gaussian with a standard deviation of $\sqrt{N}$. To guarantee a legal output density matrix, the negative eigenvalues in the linear-least-squares output are truncated [16]. This linear technique provides answers within a statistical error of an equivalent maximum likelihood-based reconstruction, but in approximately 1/1000th of the time. Thus it is suitable for near-real-time tomographic reconstruction.

We recorded a series of measurements in each of the nine different bias phase pairs. At each setting, the system measured 5×10^9 gates, with the data recorded in fifty batches of 10^8 gates each. Figure 4 shows a sample tomography analysis of our results using all the measurements. The raw fidelity is 87.3%, but after subtracting all accidental coincidence counts the fidelity increases to 97.9%. Some of the accidental counts are due to detector dark counts while others are due to issues in the entangled photon source, such as spontaneously generated Raman photons or multipair entangled photon production. The detector dark count probabilities from the six detectors were measured to be in the range of 1×10^{-5} to 6×10^{-5} per gate. Subtracting out the impact of these dark counts from the raw data leads to a dark count subtracted fidelity of 91.4%. This suggests that dark counts are a substantial part but not the only important component of the observed fidelity degradation due to accidental counts.

The measurements of Fig. 4 were recorded with after-pulse masking turned on. After-pulse masking essentially ignores

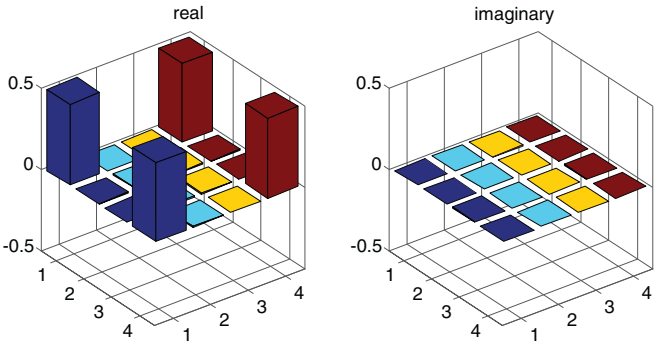

FIG. 4. (Color online) Tomography density matrix of the entire data set after accidental coincidence counts are subtracted. The corresponding fidelity is 97.9%.

detection events that occur in consecutive time bins in a given detector. We have observed that after-pulse masking can account for a small improvement in accidental-count subtracted fidelity but has negligible effect on the raw fidelity. The after-pulse count rate on the detectors when operated without after-pulse masking is typically 1 to 4%.

The data can also be processed using the interim measurements in 100 million (M) gate increments where a varying number of the interim measurements are accrued. This allows the impact of measurement time to be quantified. Figure 5(a) shows the raw and accidental count subtracted fidelities as a function of the total number of gates processed. We calculate the fidelity for cases where data from all nine bias phase pairs are used as well as when using data from a single bias phase pair. When using 100 M gates from a single bias phase pair (25 M entangled states measured), the raw fidelity is $82.2 \pm 4.6\%$, where the error bar is the standard deviation of the 450 different 100 M gate measurements (50 such measurements for each of the nine different phase bias pairs). This result is well into the quantum regime and represents a measurement time of ~2.1 s. The fastest previously reported time-bin tomography measurement reached 86% fidelity after 240 s of measurement time [12] (not including the time to change bias phases), which we accomplish in this data set after about 10 s using only a single bias phase setting.

The tomographic fidelity is slightly better when using all nine bias phase pairs, even for the same total number of gates, because the redundant measurement configuration can make the reconstruction more robust to certain nonidealities [6]. One example of such a nonideality is the combination phase of the 3×3 couplers which nominally combine the inputs with a 120° relative phase, but small variations that may occur in practice will affect the single bias phase measurement more than the nine bias phase measurement configuration. Redundant measurements can detect and/or correct for certain systematic errors in QST systems [4]. Another reason more bias phase pairs could lead to higher quality measurements is that the relative detection efficiencies of the various detectors, calculated during the tomography process, are more accurate when all nine bias phase pairs are employed. We tried using the more accurate relative detector efficiencies calculated over the entire nine bias phase pairs when processing the single bias phase pair tomography, but found the resulting

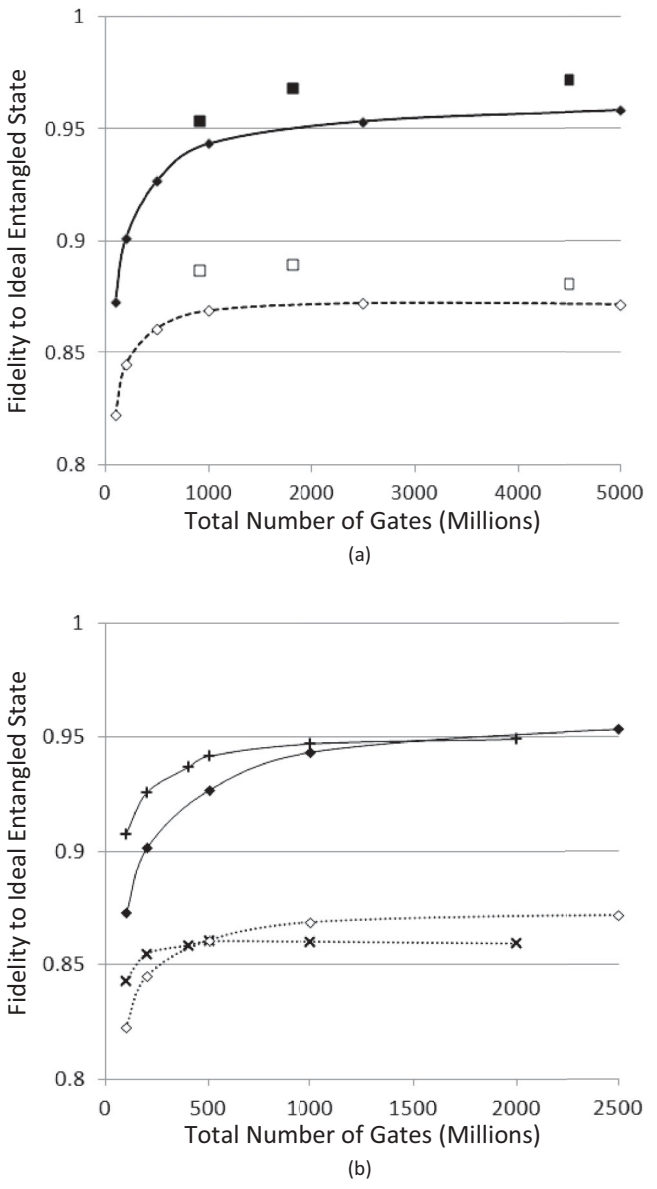

FIG. 5. Fidelity as a function of the number of processed gates. (a) The diamonds designate data processed using one bias phase pair and the squares using all the bias phase pairs. Filled markers are accidental count subtracted and unfilled are raw fidelity. (b) Single bias phase results at two different pump power levels. Diamonds are the same as in (a) while crosses and ×'s are the accidental-count subtracted data and the raw data, respectively, at a higher pump power level.

improvement to be inconsequential. This is indicative of the fairly symmetric input state being measured (maximally entangled state) allowing a single bias phase pair to adequately determine the relative detection efficiencies. Note that if a highly nonmaximally entangled state was to be measured, a single bias phase pair would not result in accurate relative detection efficiencies and some other method of calibrating the detection efficiency would be required.

Figure 5(b) compares the single bias phase measurements from the previous data set to a second data set taken with a higher pump power driving the entangled source. The original data set generated an average of 29.2 coincidence counts per

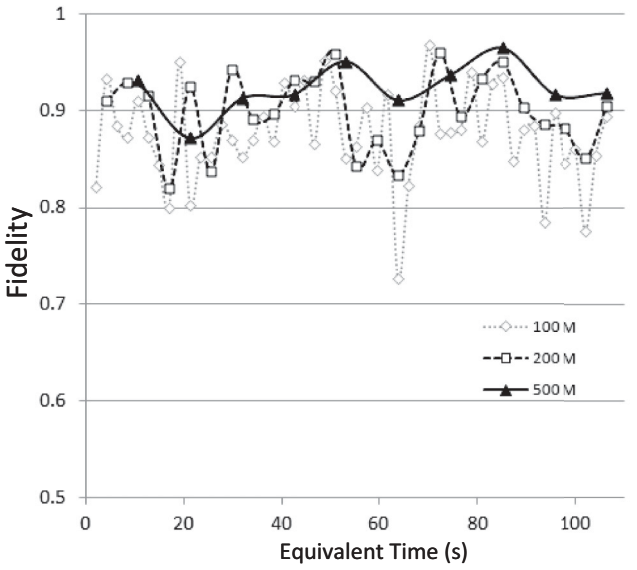

FIG. 6. Accidental count subtracted fidelity for a single bias phase pair setting as a function of equivalent time when processing gates in 100 M, 200 M, or 500 M blocks.

1 M gates, while the second data set generated 80.9 coincidence counts per 1 M gates. A plot of the fidelity as a function of gates shows that pumping at a higher power yields better performance for short measurement times where the benefit from the added number of coincidence counts outweighs the detriment of multipair production [17]. For instance, with just 100 M gates (2.1 s measurement), the higher pump power leads to a raw fidelity of $84.3 \pm 2.8\%$ and an accidental count subtracted fidelity of $90.8 \pm 3.3\%$. Longer term measurements show a better raw fidelity at the lower pump power since there are fewer multipair and Raman scattered photons to degrade the measurement. Accidental count subtracted performance is nearly the same for both cases once sufficient coincident count statistics are measured. This is expected since in this case the unwanted counts generated due to the higher pump power are subtracted out. Accidental-subtracted measurements are thus a good way to determine the quality of the measurement apparatus as opposed to the source itself. However, all the fidelities are calculated with respect to an ideal entangled state so some of the entangled source imperfections like an unbalanced pulse level in the pump time slots will also influence the accidental count subtracted fidelity.

Figure 6 replots data from the same measurement set as Fig. 5(a), but where a single phase bias setting is chosen and the same data is plotted when processed in varying block lengths. Each point thus represents a measurement over a given time interval; for instance, about 2.1 s separates each point that processes 100 M gates while 10.6 s separates each point when 500 M gates are processed. The plots thus show how the fidelity measurement changes over time, and the tradeoff between update rate and measurement variance. The fidelity measurement does not appear to have a systematic time drift indicating a stable generation and measurement system.

We note that recent research has demonstrated high speed gated detectors that can be operated at rates approaching 2 GHz with detection efficiencies above 10% [17,18]. The

detectors used in the experiment reported on here operates at 47 MHz with nominal efficiencies of ∼20%. Since the coincidence count rate is linearly proportional to the gate rate and proportional to the detection efficiency squared, we expect that reengineering this system using such 2 GHz detectors should increase the measurement speed by about one order of magnitude, allowing for effectively real-time monitoring of the fidelity of time-bin-entangled sources.

IV. CONCLUSION

We have described and experimentally demonstrated a fast time bin entanglement generation and measurement system that can perform quantum state reconstruction using a single bias phase pair setting of the signal and idler interferometers. The interferometers make use of 3×3 output couplers and all the pulses on all the output ports are measured with single photon detectors. A ditherless phase locking method is used which allows for convenient fiber-based asymmetric interferometers to be used. We have quantified the performance improvements observed when measurements are made at redundant interferometer bias phase pair settings, and have observed a 97.9% accidental-count subtracted fidelity for long term measurements that use nine different bias phase pairs. The performance improvement using nine different bias phase pairs is incremental to the single bias phase case if the relative detection efficiencies of the single photon detectors are well calibrated. When measuring symmetric states, such as nearly maximally entangled states, a single phase bias setting allows for adequate determination of the relative detection efficiencies. This leads to fast measurement times by eliminating the need to cycle through different phase bias pairs.

Raw tomographic fidelity (with respect to an ideal entangled state) of 84% with a corresponding accidental-count subtracted fidelity of >90% are recorded in a ∼2 s measurement time. Previous time-bin tomographies of similar quality used recording times several minutes long. We estimate that by incorporating the latest high speed photon counters that tomography rates of several hertz with similar performance should be possible. The results support the development of quantum measurement instrumentation with real time update rates.

ACKNOWLEDGMENT

This work was funded by DARPA on Contract No. W91CRB-10-C-0067.

[1] J. Fan, M. D. Eisaman, and A. Migdall, Opt. Express **15**, 18339 (2007).
[2] H. Hübel, M. R. Vanner, T. Lederer, B. Blauensteiner, T. Lorünser, A. Poppe, and A. Zeilinger, Opt. Express **15**, 7853 (2007).
[3] A. G. White, D. F. V. James, P. H. Eberhard, and P. G. Kwiat, Phys. Rev. Lett. **83**, 3103 (1999).
[4] M. Brodsky, E. C. George, C. Antonelli, and M. Shtiaf, Opt. Lett. **36**, 43 (2011).
[5] J. B. Altepeter, N. N. Oza, M. Medić, E. R. Jeffrey, and P. Kumar, Opt. Express **19**, 26011 (2011).
[6] J. B. Altepeter, E. R. Jeffrey, P. G. Kwiat, S. Tanzilli, N. Gisin, and A. Acin, Phys. Rev. Lett. **95**, 033601 (2005).
[7] J. B. Altepter, E. R. Jeffrey, and P. G. Kwiat, Adv. At. Mol. Opt. Phys. **52**, 105 (2005).
[8] M. Nielsen and I. Chuang, *Quantum Computation and Quantum Information* (Cambridge University Press, Cambridge, 2000).
[9] C. Z. Peng, J. Zhang, D. Yang, W. B. Gao, H. X. Ma, H. Yin, H. P. Zeng, T. Yang, X. B. Wang, and J. W. Pan, Phys. Rev. Lett. **98**, 010505 (2007).
[10] J. D. Franson, Phys. Rev. Lett. **62**, 2205 (1989).
[11] J. Brendel, N. Gisin, W. Tittel, and H. Zbinden, Phys. Rev. Lett. **82**, 2594 (1999).
[12] H. Takesue and Y. Noguchi, Opt. Express **17**, 10976 (2009).
[13] F. Bussières, J. A. Slater, J. Jin, N. Godbout, and W. Tittel, Phys. Rev. A **81**, 052106 (2010).
[14] W. Tittel, J. Brendel, H. Zbinden, and N. Gisin, Phys. Rev. Lett. **84**, 4737 (2000).
[15] H. Takesue and K. Inoue, Phys. Rev. A **72**, 041804 (2005).
[16] M. S. Kaznady and D. F. V. James, Phys. Rev. A **79**, 022109 (2009).
[17] H. C. Lim, A. Yoshizawa, H. Tsuchida, and K. Kikuchi, Opt. Express **16**, 12460 (2008).
[18] N. Namekata, S. Adachi, and S. Inoue, Photon. Tech. Lett. **22**, 529 (2010).